Robotics and Autonomous Systems 59 (2011) 711–726

Contents lists available at ScienceDirect

Robotics and Autonomous Systems

journal homepage: www.elsevier.com/locate/robot

Robust tube-based predictive control for mobile robots in off-road conditions

Ramón González [a,*], Mirko Fiacchini [b], José Luis Guzmán [a], Teodoro Álamo [c], Francisco Rodríguez [a]

[a] Dep. Lenguajes y Computación, University of Almería, Almería, Spain
[b] Laboratory for Analysis and Architecture of Systems, Toulouse, France
[c] Dep. Ingeniería de Sistemas y Automática, University of Seville, Seville, Spain

ARTICLE INFO

Article history:
Received 28 January 2011
Received in revised form
7 May 2011
Accepted 16 May 2011
Available online 30 May 2011

Keywords:
Autonomous mobile robot
Robustness
Model Predictive Control
Slip

ABSTRACT

This paper focuses on the design of a tube-based Model Predictive Control law for the control of constrained mobile robots in off-road conditions with longitudinal slip while ensuring robustness and stability. A time-varying trajectory tracking error model is used, where uncertainties are assumed to be bounded and additive. The robust tube-based MPC is compared with other motion control techniques through simulation and physical experiments. These tests show the satisfactory behavior of the presented control strategy.

1. Introduction

Mobile robotics comprises an important field of application for many control techniques, mainly those related to handle constraints (i.e., physical limitations of actuators, narrow workspaces, etc.), and uncertainties (i.e., unmodeled dynamics, simplified models, noisy measurements, etc.). Model Predictive Control (MPC) is a popular control technique to deal with constrained systems [1–3]. However, in order to tackle uncertainty, robust MPC formulations such as Min–Max MPC [4], or feedback MPC [5] must be considered.

In addition, another fundamental factor that can affect the performance of the motion of off-road mobile robots is the slip effect. Slip induces traction/velocity loss during the robot motion, which can adversely influence the mobility and controllability [6,7]. Slip can be presented in lateral and longitudinal directions. In the case of wheeled robots, lateral slip occurs due to the deformation of the pneumatic tire surface and large centrifugal force [8]. Longitudinal slip comes from pneumatic tire compression due to load on the robot. In the case of tracked robots, lateral slip is only presented at high velocity turns and it only depends on centrifugal force [9,10]. Longitudinal slip is mainly caused by the track/soil interaction, such as the sinkage effect. This produces a bulldozing phenomenon that makes the robot sinks in the soil (particularly on sandy soils) [6,10].

In the past few years, some research efforts have been devoted to the application of predictive control in mobile robotics and some of them related to off-road robots. For instance, in [9], the authors use an MPC controller to enable both anticipation of approaching curvature and to compensate from lateral slip phenomena for path tracking control of an agricultural vehicle. In [11], an MPC is applied to the trajectory tracking problem. The control law is analytically derived, which permits its application to a physical mobile robot. In order to avoid vehicle slip, velocity and acceleration are bounded. The work [12] presents a predictive strategy that permits to avoid unexpected static obstacles in the robot environment. For the purpose of MPC real-time implementation, a neural network was trained. A Smith-predictor-based generalized predictive controller is discussed in [13]. This control strategy permits dealing with dead-time uncertainties related to a mobile robot control motion.

Generally, the main issue of robust MPC strategies, which sometimes prevent its physical application, is related to the high computation burden [3,14]. Recently, an efficient theoretical concept, called "tube-based MPC", has been applied to robustify MPC [15,16]. The term tube-based refers to those control techniques whose objective is to maintain all the possible trajectories of an uncertain system inside a sequence of admissible regions. These regions are determined by taking constraints satisfaction into account. In the MPC context, the possible trajectories form a sequence of sets in the state space, which is the admissible set for each step within the prediction horizon.

The main contribution of this paper is the adaptation and application of a robust tube-based MPC strategy to the mobile robotics field. From the theoretical point of view, an extension

* Corresponding author. Tel.: +34 950214535.
E-mail addresses: rgonzalez@ual.es (R. González), fiacchini@laas.fr (M. Fiacchini), joguzman@ual.es (J.L. Guzmán), alamo@cartuja.us.es (T. Álamo), frrodrig@ual.es (F. Rodríguez).

0921-8890/$ – see front matter © 2011 Elsevier B.V. All rights reserved.
doi:10.1016/j.robot.2011.05.006

of tube-based predictive control to time-varying systems using reachable sets is provided. In this case, a trajectory tracking error model of a mobile robot in slip conditions is considered. In order to ensure stability, Linear Matrix Inequalities (LMI) formalism is employed to determine a Lyapunov function constituting the terminal cost, and a terminal robust positively invariant set following the ideas of Blanchini [17], and Kolmanovsky and Gilbert [18] is also calculated. Finally, the robust tube-based MPC has been compared to other motion control techniques through simulation and off-road physical experiments. These tests show the satisfactory behavior of the suggested control strategy and the efficient real-time execution. In the physical experiments, the visual odometry approach has been used for robot localization purposes.

This paper is organized as follows: Section 2 presents the problem statement. The control objective and the robust tube-based MPC control law are stated in Section 3. Section 4 shows a comparison of the proposed controller with other motion control techniques through simulation and physical experiments. Finally, Section 5 deals with conclusion and future research. Videos related to the physical experiments are available at http://www.ual.es/personal/rgonzalez/videosMPC.htm.

2. Problem statement

In this section, the time-varying trajectory tracking error model of a mobile robot in slip conditions is considered. This model is discretized and an additive uncertainty term has been included.

Trajectory tracking consists in the problem in which a robot must follow a *reference or virtual* mobile robot representing the desired positions and velocities [19]. Hence, the objective is to find a feedback control law such that the error between the desired location and the real location of the mobile robot approaches zero (regulation problem).

These errors are expressed in the real robot frame as

$$\begin{bmatrix} e_x(t) \\ e_y(t) \\ e_\theta(t) \end{bmatrix} = \begin{bmatrix} \cos(\theta^{sl}(t)) & \sin(\theta^{sl}(t)) & 0 \\ -\sin(\theta^{sl}(t)) & \cos(\theta^{sl}(t)) & 0 \\ 0 & 0 & 1 \end{bmatrix} \begin{bmatrix} x^{rf}(t) - x^{sl}(t) \\ y^{rf}(t) - y^{sl}(t) \\ \theta^{rf}(t) - \theta^{sl}(t) \end{bmatrix}, \tag{1}$$

where $t \in \mathbb{R}^+$ is the continuous time, $e_x \in \mathbb{R}$ is the longitudinal error, $e_y \in \mathbb{R}$ is the lateral error and $e_\theta \in \mathbb{R}$ is the orientation error. The rest of terms are defined in what follows.

In this work, the reference robot is defined by the kinematic model of a differential-drive robot [20]

$$\begin{aligned} \dot{x}^{rf}(t) &= \frac{v_r^{rf}(t) + v_l^{rf}(t)}{2} \cos\theta^{rf}(t), \\ \dot{y}^{rf}(t) &= \frac{v_r^{rf}(t) + v_l^{rf}(t)}{2} \sin\theta^{rf}(t), \\ \dot{\theta}^{rf}(t) &= \frac{v_r^{rf}(t) - v_l^{rf}(t)}{b}, \end{aligned} \tag{2}$$

where $[x^{rf}\ y^{rf}\ \theta^{rf}]^T \in \mathbb{R}^3$ represents the location (position and orientation) of the reference mobile robot, $v_r^{rf} \in \mathbb{R}^+$ and $v_l^{rf} \in \mathbb{R}^+$ are the reference linear velocities of right and left wheels, respectively, and $b \in \mathbb{R}$ is the distance between the wheel centers.

Assumption 1. Assume that reference robot wheel velocities are known positive ($v_r^{rf} > 0$, $v_l^{rf} > 0$) and bounded ($v_r^{rf} \in [v_r^{rf,m}, v_r^{rf,M}]$, $v_l^{rf} \in [v_l^{rf,m}, v_l^{rf,M}]$).

On the other hand, the real robot is modeled taking into account an extended kinematic model where some terms related to longitudinal slip appear. Such kinematic model is given by [10,21]

$$\begin{aligned} \dot{x}^{sl}(t) &= \frac{v_r^{sl}(t) + v_l^{sl}(t)}{2} \cos\theta^{sl}(t), \\ \dot{y}^{sl}(t) &= \frac{v_r^{sl}(t) + v_l^{sl}(t)}{2} \sin\theta^{sl}(t), \\ \dot{\theta}^{sl}(t) &= \frac{v_r^{sl}(t) - v_l^{sl}(t)}{b}, \end{aligned} \tag{3}$$

where $[x^{sl}\ y^{sl}\ \theta^{sl}]^T \in \mathbb{R}^3$ represents the location of the mobile robot, and

$$\begin{aligned} v_r^{sl}(t) &= v_r(t)\big(1 - i_r(t)\big), \\ v_l^{sl}(t) &= v_l(t)\big(1 - i_l(t)\big), \end{aligned} \tag{4}$$

where $v_r^{sl} \in \mathbb{R}$ and $v_l^{sl} \in \mathbb{R}$ are the linear velocities taking into account slip effects, $v_r \in \mathbb{R}$ and $v_l \in \mathbb{R}$ are the linear velocities of the right and left wheels, respectively, and $i_r \in \mathbb{R}^+$ and $i_l \in \mathbb{R}^+$ are the terms representing the longitudinal slip component. Note that, by definition, $i_r, i_l \in [0, 1)$, for details see [6,21].

Assumption 2. It is assumed that the real mobile robot moves at low velocities ($\leq$2 (m/s)).

Remark 1. Note that from Assumption 2, lateral slip and forces arising from dynamic effects are neglected. As stated in [10,22], lateral slip is zero for straight-line motions and it can be neglected when the vehicle turns "on the spot" or at low velocities. However, longitudinal slip is an unavoidable effect of the robot-terrain interaction [6].

As shown in [21], differentiation of Eq. (1) with respect to time and defining the following virtual control signals for linearization purposes

$$u_1(t) = -v^{sl}(t) + v^{rf}(t), \tag{5}$$

$$u_2(t) = -\dot{\theta}^{sl}(t) + \dot{\theta}^{rf}(t), \tag{6}$$

where $v^{sl} = (v_r^{sl} + v_l^{sl})/2$ is the linear velocity of the robot taking into account slip effects and $v^{rf} = (v_r^{rf} + v_l^{rf})/2$ is the linear velocity of the reference. Previous process leads to the following linear, time-varying, discrete-time system

$$e(k+1) = A_{\gamma(k)}e(k) + B_d u(k) + w(k), \tag{7}$$

where $k \in \mathbb{Z}^+$ is the discrete time, $e = [e_x\ e_y\ e_\theta]^T \in \mathbb{R}^3$ is the current state (error), $u = [u_1\ u_2]^T \in \mathbb{R}^2$ is the current input (see Remark 2), and w is a bounded additive uncertainty satisfying $w \in W$, where W is a polytope in the state space $\mathbb{R}^3$ (see Remark 3). The matrices A_γ and B_d are defined as

$$A_{\gamma(k)} = \begin{bmatrix} 1 & \epsilon(k) & 0 \\ -\epsilon(k) & 1 & \rho(k) \\ 0 & 0 & 1 \end{bmatrix}, \qquad B_d = \begin{bmatrix} T_s & 0 \\ 0 & 0 \\ 0 & T_s \end{bmatrix}, \tag{8}$$

where $\epsilon = T_s\left(\frac{(1-\bar{i}_r)v_r^{rf} - (1-\bar{i}_l)v_l^{rf}}{b}\right)$ and $\rho = T_s v^{rf}$, $T_s \in \mathbb{R}^+$ is the sampling time, and $\bar{i}_r \in \mathbb{R}^+$ and $\bar{i}_l \in \mathbb{R}^+$ are the nominal slip of each wheel (see Remark 4). For sake of notational simplicity, the dependence of A_γ on k is omitted.

From Assumption 1, $\gamma = [v_r^{rf}\ v_l^{rf}]^T \in \mathbb{R}^2$ is a time-varying vector such that $\gamma(k) \in \Gamma$, $\forall k \in \mathbb{Z}^+$, where $\Gamma \subseteq \mathbb{R}^2$ is a polytope. For any admissible realization of parameter $\gamma \in \Gamma$, a dynamic matrix A_γ is determined. It follows that $A_\gamma \in \mathscr{A}$, with $\mathscr{A}$ being a polytope in $\mathbb{R}^{3\times3}$ that represents the dynamic system matrix.

Remark 2. Note that according to (5)–(6), the linear velocities for each wheel are obtained as

$$v_r(t) = \frac{v_r^{rf}(t) - u_1(t) - \frac{b}{2}u_2(t)}{1 - i_r(t)}, \tag{9}$$

$$v_l(t) = \frac{-v_l^{rf}(t) + u_1(t) - \frac{b}{2}u_2(t)}{-1 + i_l(t)}, \tag{10}$$

where $v_r \in [v_r^m, v_r^M]$ and $v_l \in [v_l^m, v_l^M]$. This leads to bounds on the space of u, which are obtained from the constraints on $v_r, v_l, i_r, i_l, v_r^{rf}, v_l^{rf}$.

Remark 3. The set $W \subseteq \mathbb{R}^3$ represents the uncertainty affecting the state at each sampling instant. This uncertainty bounds the mismatch between the continuous-time non-linear trajectory tracking error model and the discrete-time linear model, the noise in the slip estimation, and the uncertainty in the robot localization. In this case, such mismatch has been estimated simulating random input values to both models. Furthermore, the set W has been enlarged to take into account both the noise in the slip estimation and the uncertainty in the robot localization based on physical experiments (estimating the deviation between the robot localization and the ground-truth through several physical experiments).

Remark 4. Notice that the nominal slip in the model is used, since the real values of i_r and i_l are not known for the predictions.

Finally, the states and inputs are subject to the following constraints

$$e(k) \in E, \qquad u(k) \in U, \tag{11}$$

where $E \subseteq \mathbb{R}^3$ and $U \subseteq \mathbb{R}^2$ are polytopes that contain the origin. Recall that state and input constraints represent the physical limitations such as narrow spaces of operation and saturations on the actuators of the problem.

2.1. Definitions

A *polyhedron* is the (convex) intersection of a finite number of open and/or closed half-spaces and a *polytope* is a closed and bounded polyhedron. The *convex hull* of a set of points is defined as the smallest convex set containing the points, and it is denoted as *co*. Given two sets $X, Y \subseteq \mathbb{R}^n$, the Minkowski sum is defined by $X \oplus Y \triangleq \{x + y \mid x \in X, y \in Y\}$ and the Pontryagin set difference is $X \ominus Y \triangleq \{x \mid x \oplus Y \subseteq X\}$. For a given $\lambda \geq 0$, $\lambda X = \{\lambda x : x \in X\}$.

3. Robust MPC strategy

In this section, the implementation of the robust tube-based MPC is discussed, adapting the ideas of Chisci et al. [15], and Langson et al. [16]. First, a local control law that compensates the effect of uncertainty is calculated. This leads to reachable sets containing the real state for every possible realization of the uncertainty and every admissible parameter occurrence. Finally, as explained in [15], online computation is only devoted to the solution of a deterministic MPC for a nominal system with restricted constraints (see Fig. 1).

The nominal system is defined as

$$\tilde{e}(k+1) = A_\gamma \tilde{e}(k) + B_d g(k), \tag{12}$$

where $\tilde{e} \in \mathbb{R}^3$ is the nominal state, and $g \in \mathbb{R}^2$ is the control input for the nominal system. Observe that this is equivalent to system (7) with $W = \{0\}$.

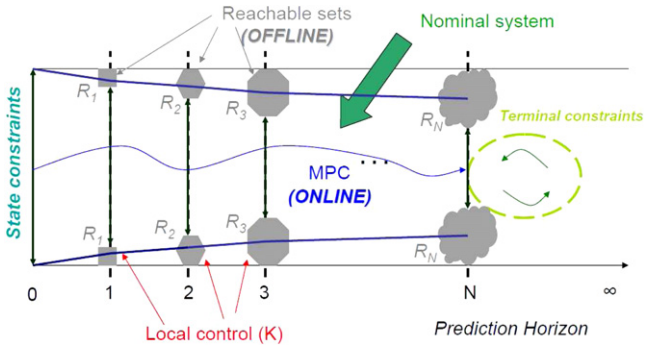

Fig. 1. Robust tube-based MPC control strategy. Reachable sets are solved offline compensating uncertainty, online computation is devoted to solve a nominal MPC.

The control objective is to design a state feedback control law of the form [15]

$$u(k) = K\bar{e}(k) + g(k), \tag{13}$$

$$\bar{e}(k) = e(k) - \tilde{e}(k), \tag{14}$$

where $K \in \mathbb{R}^{2\times 3}$ is a local controller whose goal is to compensate the mismatch between the real (7) and the nominal (12) systems, $\bar{e} = [\bar{e}_x\ \bar{e}_y\ \bar{e}_\theta]^T$ is the mismatch state vector and g is the online MPC control input.

Replacing (7) and (12) into (14), the local uncertain closed-loop system follows as

$$\bar{e}(k+1) = e(k+1) - \tilde{e}(k+1) = (A_\gamma + B_d K)\bar{e}(k) + w(k). \tag{15}$$

3.1. Control objectives

In this paper, the major control objectives are:

- Robustness: Following the tube-based MPC policy, original constraints (11) are replaced with more restricted ones, which take into account additive uncertainties and time-varying dynamics.
- Performance: An optimization problem (QP) is solved at each sampling instant obtaining the proper control actions as a compromise between small deviations from the reference trajectory and suitable control actions.
- Input and state constraints fulfillment: This requirement is guaranteed ensuring constraints satisfaction in the minimization of the MPC control law.
- Asymptotic stability: It is assured through a quadratic Lyapunov function determined using LMI and a robust positively invariant set for the terminal region of the nominal MPC.
- Efficient real-time execution: A standard nominal MPC is solved online to control the nominal system since the effect of the uncertainties and system dynamics are already included in the restricted constraints. This fact implies that the robust tube-based MPC strategy fits properly to mobile robotics applications, where high sampling frequencies are employed.

Fig. 1 summarizes the robust tube-based MPC strategy. First, the reachable sets are calculated for the local uncertain closed-loop system (15) (see Section 3.2), then the state and input constraints are replaced using the previously calculated reachable sets (Section 3.3). Finally, an MPC control law to the nominal system is applied (detailed in Section 3.4). In order to ensure the stability of the nominal MPC, a Lyapunov function and a terminal robust positively invariant set are determined (Section 3.5). We would like to point out that both reachable sets calculation and the replacement of state and input constraints are carried out offline, so they do not influence online computation burden. Online computation is only devoted to solve the standard MPC controller handling the nominal system for which tighter constraints are considered.

3.2. Local compensation of system dynamics

In this subsection, the control law that compensates the mismatch between the real and nominal systems and the reachable sets, that will be used in what follows, are calculated.

First, in order to implement the tube-based MPC, the system matrix, A_γ, is decomposed into the time-invariant and time-varying parts

$$A_\gamma = I_3 + A^r v_r^{rf} + A^l v_l^{rf}, \tag{16}$$

where $I_3 \in \mathbb{R}^{3\times 3}$ is the identity matrix, and

$$A^r = \begin{bmatrix} 0 & \xi & 0 \\ -\xi & 0 & \beta \\ 0 & 0 & 0 \end{bmatrix}, \qquad A^l = \begin{bmatrix} 0 & -\varsigma & 0 \\ \varsigma & 0 & \beta \\ 0 & 0 & 0 \end{bmatrix}, \tag{17}$$

with $\xi = T_s\left(\frac{1-\bar{i}_r}{b}\right)$, $\beta = \frac{T_s}{2}$, $\varsigma = T_s\left(\frac{1-\bar{i}_l}{b}\right)$.

From Assumption 1, it follows

$$v_r^{rf} = \bar{v}_r^{rf} + \Delta v_r^{rf} \Rightarrow \Delta v_r^{rf} \in [\delta v_r^{rf,m}, \delta v_r^{rf,M}], \tag{18}$$

$$v_l^{rf} = \bar{v}_l^{rf} + \Delta v_l^{rf} \Rightarrow \Delta v_l^{rf} \in [\delta v_l^{rf,m}, \delta v_l^{rf,M}], \tag{19}$$

where $\bar{v}_r^{rf}$ and $\bar{v}_l^{rf}$ are the reference nominal velocities of the right and left wheels, respectively, and Δv_r^{rf} and Δv_l^{rf} can be seen as the new ranges in the reference velocities. Hence, the matrix A_γ can be expressed as

$$A_\gamma = A^n + A^r \Delta v_r^{rf} + A^l \Delta v_l^{rf}, \tag{20}$$

where $A^n = I_3 + A^r \bar{v}_r^{rf} + A^l \bar{v}_l^{rf}$ represents the time-invariant part of matrix A_γ and the rest of terms are time-varying, which must be bounded. Replacing previous equation into (15), it is obtained

$$\bar{e}(k+1) = [A^n + A^r \Delta v_r^{rf} + A^l \Delta v_l^{rf} + B_d K]\bar{e}(k) + w(k). \tag{21}$$

In order to compensate the system dynamics, the local control gain K is defined as (see Remark 5)

$$K = K^n + K^r \Delta v_r^{rf} + K^l \Delta v_l^{rf}, \tag{22}$$

which implies that Eq. (21) becomes

$$\bar{e}(k+1) = A_{cl}^n \bar{e}(k) + A_{cl}^r \Delta v_r^{rf} \bar{e}(k) + A_{cl}^l \Delta v_l^{rf} \bar{e}(k) + w(k), \tag{23}$$

where $A_{cl}^n = (A^n + B_d K^n)$, $A_{cl}^r = (A^r + B_d K^r)$, and $A_{cl}^l = (A^l + B_d K^l)$.

Local controller K^n is straightforwardly obtained solving an *LQR* problem [23]. Local controllers K^r and K^l can be chosen such that the effect of the system dynamics in matrices A^r and A^l is partially compensated in closed-loop. Choosing

$$K^r = \begin{bmatrix} 0 & -\frac{\xi}{T_s} & 0 \\ 0 & 0 & 0 \end{bmatrix}, \qquad K^l = \begin{bmatrix} 0 & \frac{\varsigma}{T_s} & 0 \\ 0 & 0 & 0 \end{bmatrix}, \tag{24}$$

it is obtained that

$$A_{cl}^r = \begin{bmatrix} 0 & 0 & 0 \\ -\xi & 0 & \beta \\ 0 & 0 & 0 \end{bmatrix}, \qquad A_{cl}^l = \begin{bmatrix} 0 & 0 & 0 \\ \varsigma & 0 & \beta \\ 0 & 0 & 0 \end{bmatrix}. \tag{25}$$

Remark 5. Notice that $K = K^n + K^r \Delta v_r^{rf} + K^l \Delta v_l^{rf}$ can be seen as an adaptive local control law which tries to compensate the local mismatch system (15). However, as can be checked from (25) it is not possible to completely compensate the effects on $\bar{e}_y$, but it can be done for the components $\bar{e}_x$ and $\bar{e}_\theta$. Furthermore, K^n is chosen solving an *LQR* problem, then leading to stability of the nominal closed-loop dynamics A_{cl}^n. On the other hand, we would like to remark that K could be obtained solving online an optimization problem in terms of LMI similarly to the approach detailed in [7]. However, this issue would lead to increase the online computation burden at each step within the prediction horizon.

We have to compute the sequence of sets that can be reached by the closed-loop local uncertain system (15) iteratively with $\mathscr{R}_0 = \{0\}$ and the following iteration

$$\mathscr{R}_{j+1} \triangleq \bigcup_{A_\gamma \in \mathscr{A}} (A_\gamma + B_d K)\mathscr{R}_j \oplus W, \quad \forall j = 0, \ldots, N-1, \tag{26}$$

where $\mathscr{R}_j$ is the reachable set of the jth step in the prediction horizon N. From Remark 5, the reachable sets obtained from (26) can be computed as

$$\begin{aligned} \mathscr{R}_{j+1} = {} & A_{cl}^n \mathscr{R}_j \oplus co\{(A_{cl}^r \delta v_r^{rf,m} \mathscr{R}_j) \cup (A_{cl}^r \delta v_r^{rf,M} \mathscr{R}_j)\} \\ & \oplus co\{(A_{cl}^l \delta v_l^{rf,m} \mathscr{R}_j) \cup (A_{cl}^l \delta v_l^{rf,M} \mathscr{R}_j)\} \oplus W, \\ & \forall j = 0, \ldots, N-1. \end{aligned} \tag{27}$$

Notice that this formulation is slightly different from that exposed in [15], since now the parameter dependence of the system dynamics is taken into account in the reachable sets calculation.

3.3. Robust tube-based MPC

When dealing with uncertain systems, deterministic MPC is limited – although some degree of robustness is achieved due to feedback [24] – since the uncertainties are not explicitly considered in the synthesis of the control law to guarantee robust stability [4]. As explained above, the concept of tube-based MPC implies the replacement of the original constraints (11) with more restricted ones [15]. Following the ideas of Chisci et al., imposing that $\tilde{e}_j \in \tilde{E}_j$, $\forall j = 0, \ldots, N$, where $\tilde{E}_j$ is defined as

$$\tilde{E}_j = E \ominus \mathscr{R}_j, \quad \forall j = 0, \ldots, N-1, \tag{28}$$

then constraints satisfaction is ensured and feasibility is also preserved in the presence of uncertainties in the system (7). In addition, the input constraints are also replaced by

$$\begin{aligned} & \tilde{U}_j = U \ominus \left(K^n \mathscr{R}_j \oplus K^r \Delta v_r^{rf} \mathscr{R}_j \oplus K^l \Delta v_l^{rf} \mathscr{R}_j\right), \\ & \forall j = 0, \ldots, N-1. \end{aligned} \tag{29}$$

Remark 6. It is important to point out that reachable sets sequence carries all the information about every possible trajectory, which is a function of the realization of the uncertainty. For that reason, large system uncertainty could lead to empty or tiny restricted state and input constraints (sets $\tilde{E}_j$ and $\tilde{U}_j$). However, it is noticed that the problem of feasibility is hardly avoidable, and this fact constitutes an important issue of tube-based MPC approaches [15,16,18]. For the case under consideration, a trade-off has been realized, mainly varying the prediction horizon, in order to achieve an acceptable size of the reachable sets.

3.4. MPC strategy

Assume that a measurement of the state $\tilde{e}$ is available at the current time k. Then, the optimization problem is stated as follows [15,16]

$$\min_{G(k) \triangleq \{g_k, \ldots, g_{k+N-1}\}} \quad J_N(G(k), \tilde{e}(k)), \tag{30}$$

subject to

$$\begin{aligned} & \tilde{e}_{k+j|k} \in \tilde{E}_j && \forall j = 1, \ldots, N, \\ & g_{k+j} \in \tilde{U}_j && \forall j = 0, \ldots, N-1, \\ & \tilde{e}_{k+N|k} \in \Omega \ominus \mathscr{R}_N, \end{aligned}$$

where $\tilde{e}_{k+j|k}$ denotes the predicted state vector at time $k+j$, obtained by applying the input sequence $G(k) \triangleq \{g_k, \ldots, g_{k+N-1}\}$ to model (12) starting from the state $\tilde{e}(k)$. Notice that the MPC

includes the new state and input constraints (28)–(29). The considered cost function is given by

$$J_N(G(k), \tilde{e}(k)) = \sum_{j=0}^{N-1} \tilde{e}_{k+j|k}^T Q \tilde{e}_{k+j|k} + g_{k+j}^T R g_{k+j} + \Upsilon(\tilde{e}_{k+N|k}), \quad (31)$$

where $Q = Q^T = [q_x\ q_y\ q_\theta] I_3 \geq 0$ and $R = R^T = [r_r\ r_l] I_2 > 0$. Notice that Q, R, constitute parameters to be tuned for the MPC control law. Depending on their values more attention can be given to the states or to the control signals (see discussion in Section 4). The terminal cost $\Upsilon(\cdot)$, and the terminal constraint set given by the region Ω in (30), are both calculated as illustrated in the subsequent section.

To summarize, the MPC control law is based on the following idea [25]: At time k, compute the optimal solution $G^*(k) = \{g_k^*, \ldots, g_{k+N-1}^*\}$ to problem (30) and apply

$$u(k) = K\bar{e}(k) + g_k^* \quad (32)$$

as input to system (7); repeat the optimization (30) at time $k+1$ based on the new state $\tilde{e}(k+1)$, and continue iteratively.

3.5. Terminal constraints for nominal MPC

A common approach to ensure the stability of deterministic MPC (30) consists in incorporating both a terminal cost, Υ, and a terminal constraint set, Ω [1]. Notice that we are ensuring asymptotic stability for nominal MPC. The stability for the overall controlled system is not demonstrated since it is beyond the scope of the paper. Stability for similar approaches is demonstrated in [15,26].

The purpose of the terminal cost is to ensure closed-loop stability. To this end, it requires the use of a Lyapunov function with a stabilizing control law. In this case, given a quadratic function $\Upsilon(\tilde{e}) = \tilde{e}^T P \tilde{e}$, the stability of the system is guaranteed if there exists a matrix $P > 0$ such that $\Upsilon(\tilde{e}(k+1)) - \Upsilon(\tilde{e}(k)) < 0$, for all $\tilde{e}(k) \neq 0$ (*Lyapunov function*) [27,28].

Using the LMI formulation [27,28] to obtain matrix P and optimizing with respect to the *LQR*, the following inequality is defined

$$\tilde{e}^T((A_{cl}^i)^T P A_{cl}^i)\tilde{e} - \tilde{e}^T P \tilde{e} \leq \tilde{e}^T(-Q - (\kappa^i)^T R \kappa^i)\tilde{e}, \quad \forall i = 1, \ldots, n_\gamma. \quad (33)$$

Notice that the previous inequality is only imposed at the extremal values of the polytopic set Γ, i.e. at the $n_\gamma = 2^2$ vertices of Γ. It can be proved that the fulfillment of such conditions at the vertices yields the satisfaction at any point in Γ [7].

The closed-loop matrices A_{cl}^i are given by

$$A_{cl}^i = A^i + B_d \kappa^i, \quad \forall i = 1, \ldots, n_\gamma, \quad (34)$$

where κ^i are the gains ensuring the stability of the closed-loop system, and

$$A^1 = (A^n + A^r \delta v_r^{rf,m} + A^l \delta v_l^{rf,M}), \quad (35)$$

$$A^2 = (A^n + A^r \delta v_r^{rf,m} + A^l \delta v_l^{rf,m}), \quad (36)$$

$$A^3 = (A^n + A^r \delta v_r^{rf,M} + A^l \delta v_l^{rf,m}), \quad (37)$$

$$A^4 = (A^n + A^r \delta v_r^{rf,M} + A^l \delta v_l^{rf,M}). \quad (38)$$

Using (33) and applying the Schur complement [27], it becomes

$$\begin{bmatrix} P - Q - (\kappa^i)^T R \kappa^i & (A_{cl}^i)^T \\ A_{cl}^i & P^{-1} \end{bmatrix} \geq 0, \quad (39)$$

for the ith vertex. From previous inequality, it holds

$$\begin{bmatrix} P & (A_{cl}^i)^T & Q^{\frac{1}{2}} & (\kappa^i)^T R^{\frac{1}{2}} \\ A_{cl}^i & P^{-1} & 0 & 0 \\ Q^{\frac{1}{2}} & 0 & I & 0 \\ R^{\frac{1}{2}} \kappa^i & 0 & 0 & I \end{bmatrix} \geq 0, \quad (40)$$

for the ith vertex, with I being the identity matrix. Now, pre- and post-multiplying by

$$\begin{bmatrix} P^{-1} & 0 & 0 & 0 \\ 0 & I & 0 & 0 \\ 0 & 0 & I & 0 \\ 0 & 0 & 0 & I \end{bmatrix}, \quad (41)$$

and replacing $S = P^{-1}$, $Y^i = \kappa^i P^{-1}$, and $A_{cl}^i = A^i + B_d \kappa^i$, it is obtained

$$\begin{bmatrix} S & S(A^i)^T + (Y^i)^T B_d^T & SQ^{\frac{1}{2}} & (Y^i)^T R^{\frac{1}{2}} \\ A^i S + B Y^i & S & 0 & 0 \\ Q^{\frac{1}{2}} S & 0 & I & 0 \\ R^{\frac{1}{2}} Y^i & 0 & 0 & I \end{bmatrix} \geq 0. \quad (42)$$

Then, the optimization problem to be solved is given by

$$\begin{array}{ll} \min\limits_{S>0,\ Y^i \forall i} & \mathrm{Tr}(P) \\ \text{subject to} & (42) \quad \forall i, i = 1, \ldots, 4, \end{array} \quad (43)$$

where $\mathrm{Tr}(\cdot)$ denotes the trace of a matrix [27]. The solution of this optimization problem produces four gains $(\kappa^1, \kappa^2, \kappa^3, \kappa^4)$ and the matrix P which defines the terminal cost.

Finally, in order to calculate the terminal region Ω as a robust positively invariant set for the system, the ideas in [17,18] have been adapted to this particular case. Details are presented in Appendix.

4. Results and discussion

The aim of this section is to validate the performance of the robust tube-based MPC control law and to compare it with existing time-varying control techniques. In this case, the well-known linear time-varying controller described in [19] has been implemented (denoted in figures as "No slip comp."). Furthermore, in order to compare the new proposed formulation with a controller that compensates slip effects, the work presented in [21] has also been considered (referred to as "Slip comp." in figures). This control strategy constitutes an easy extension of the former feedback control law, but now slip explicitly appears as a parameter in determination of the feedback gains. For details about this strategy, see [21]. The reference trajectories have been calculated based on unicycle kinematics.

Simulations have been carried out in Matlab® suite using the LMI toolbox [29] and MPT toolbox [30]. Physical experiments were programmed using LabVIEW® and Matlab®.

Some tuned parameters used for simulation and physical experiments are: $b = 0.5$ (m), $T_s = 0.35$ (s), and $N = 5$. This prediction horizon has been selected as a trade-off between satisfactory performance and an acceptable size of the reachable sets (see Remark 6).

As commented in Section 3.4, the values of matrices Q and R influence the performance of the MPC controller. For that reason, an important trade-off has been carried out to obtain the proper values. The most interesting conclusions are:

- For small values of q_θ and r_l (<1), the controller achieves small deviations in longitudinal and lateral directions, but not appropriate orientation error and oscillatory signals.

- Large values of q_θ and r_l (>10) produce a large error in the longitudinal direction and in the orientation, and a really oscillatory behavior in the control signals.
- Values of q_θ smaller than 1 and $R = I_2$ yield a satisfactory error in robot orientation and satisfactory control signals.

Therefore, $Q = \text{diag}([1\ 1\ 0.0001])$ and $R = I_2$ have been chosen in order to obtain an appropriate performance, small errors and smooth control signals. The sampling period has been empirically selected taking into account the desired closed-loop performance. The parameters of the two selected controllers are $\beta_c = 1$ and $\delta_c = 0.6$ to reach a soft overdamped closed-loop behavior. For more details about these parameters see [19,21].

4.1. Experimental mobile robot

The vehicle under consideration is a TMR available at the University of Almería (Spain) called *Fitorobot*, which has been used as the testbed in this work (see Fig. 2). This TMR has been designed to operate inside greenhouses for spraying purposes. As presented in [31], greenhouse terrain is composed of loose sandy soils, which can produce significant slip phenomena in vehicles. Furthermore, greenhouses are characterized by narrow corridors between plants, in which this robot has to operate. Hence, hard constraints satisfaction becomes an essential factor of the robust control problem, that means, small lateral error should be ensured to avoid that the robot collides with the plants.

The mobile robot has a mass of 500 (Kg) and its dimensions are 1.5 (m) long $\times$ 0.7 (m) wide. It is driven by a 20 (HP) gasoline engine. More details about the TMR can be found in [31].

4.2. Simulations

In this subsection, some simulations carried out before the physical experiments are detailed. Due to the complexity of the physical system (track-soil interactions, resistance forces, inertia forces, etc.), the kinematic models have been simulated. However, to make more realistic simulations, a small random noise (Gaussian distributed noise) was added to the states.

In order to check the robustness of the controllers, nominal slip for each wheel is set to[1] 10 (%), and it is supposed that slips vary within ± 15 (%). The uncertainty set is given by[2] $W = \{w_1, w_2 \in \pm 0.0035\ (\text{m}), w_3 \in \pm 0.25\ (\text{deg})\}$. State constraints are $E = \{e_x, e_y \in \pm 0.5\ (\text{m}), e_\theta \in \pm 20\ (\text{deg})\}$ and reference linear wheel velocities are restricted to $\{v_r^{rf}, v_l^{rf} \in [0.1, 1.4]\ (\text{m/s})\}$. Real linear track velocities were also experimentally determined as $\{v_r, v_l \in [-2, 2]\ (\text{m/s})\}$. In all cases, the initial location of the mobile robot was the same that the reference.

Although many trajectories have been tested, a reference trajectory that comprises the full reference velocity range has been tested. In this case, the reference velocities are always changing between the bounds and never become constant. The total traveled distance is close to 70 (m). As depicted in Fig. 3(b), slips have been simulated between 0–25(%), and reference velocities vary between 0.1–1.4 (m/s).

Fig. 3(a) shows the reference trajectory and the followed trajectories using the three compared control strategies. In this case, the predictive controller fixes properly the reference.

The errors between the reference trajectory and those steered by the compared controllers are displayed with respect to the traveled distance in Fig. 4. Notice that, although a small random noise was added to the states, the MPC controller achieves an almost zero error in the longitudinal and lateral directions and a maximum orientation error of 0.80 (deg). The rest of controllers have a maximum lateral error of -0.10 (m) for the slip compensation controller, and -0.34 (m) for the no slip compensation controller; a maximum longitudinal error of 0.07 (m) for the slip compensation controller, and 0.27 (m) for the no slip compensation controller, and finally, a maximum orientation error of -3.16 (deg) for the slip compensation controller, and -13.78 (deg) for the no slip compensation controller.

Fig. 2. Tracked mobile robot *Fitorobot* in the experiment site.

Fig. 5 displays the control inputs or linear velocities of the wheels. Notice the non-static reference velocities comprising all the range, that is, from 0.1 to 1.4 (m/s). In this figure, it can be observed how controllers compensate the effect of slip, that is, since slip decreases the velocity of the wheels, the motion controllers increase the set-points in order to compensate such negative effect. In this figure, it is possible to observe the oscillatory control actions generated by the no slip compensation controller. For instance, at sampling instant 45 (s) for the right track and at sampling instant 27 (s) for the left track.

As commented in Remark 6, restricted state and input constraints are not empty or tiny for the proposed control law. In Fig. 6, the state constraints and the terminal robust positively invariant set are shown.

4.3. Physical experiments

In this subsection, the results of the physical experiments carried out using the real mobile robot are presented. Before discussing these experiments, some considerations about practical issues are pointed out:

- A typical four-layer navigation architecture [32] has been designed and implemented in order to attempt physical experiments (see Fig. 7). The first layer is devoted to path planning. The second layer includes the motion controller presented in this paper. In the third layer, two low-level controllers have been implemented in order to ensure that the set-points generated by the motion controllers are reached by the robot tracks. For that purpose, two PI controllers with an anti-windup scheme have been tuned. The fourth layer is related to the robot localization.

[1] Notice that, for notational convenience, slip is shown in percent.

[2] Recall that W represents the uncertainty on the state for each time instant. In particular, it bounds the mismatch between the continuous-time non-linear trajectory tracking error model and the discrete-time linear model, the noise in the slip estimation, and the uncertainty in the robot localization. These values were obtained experimentally. Then, a value of $w_1 \in \pm 0.0035$ (m) represents an uncertainty in the e_x state of ± 1 (cm) each second.

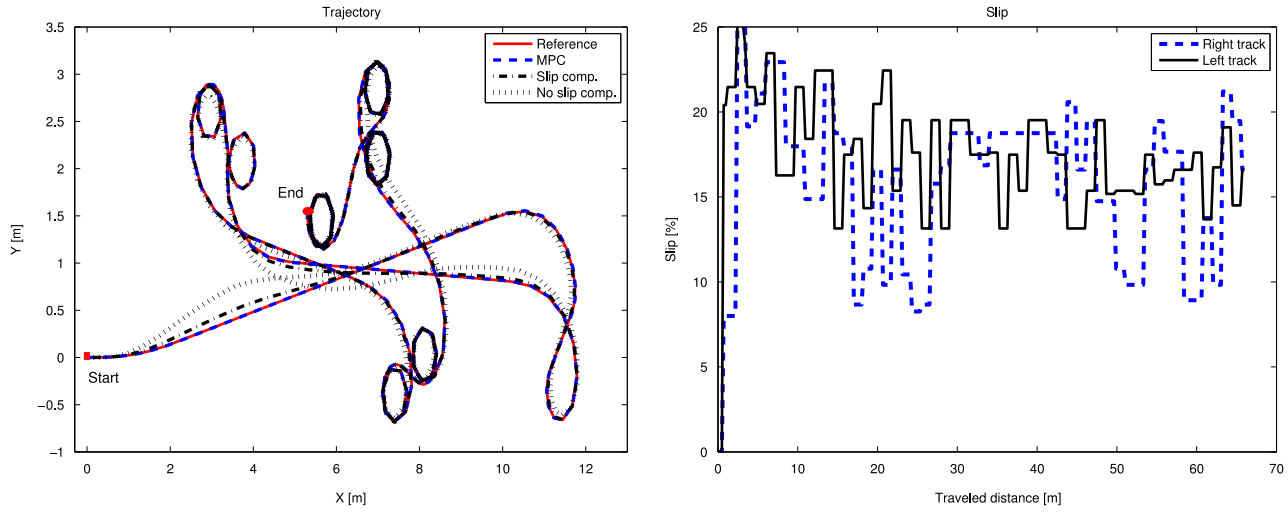

(a) Followed trajectories.

(b) Simulated slip profiles.

Fig. 3. Tracked trajectories and slip profiles. Reference trajectory is generated supposing an unicycle model. Slip has been simulated similar to that found in real tests.

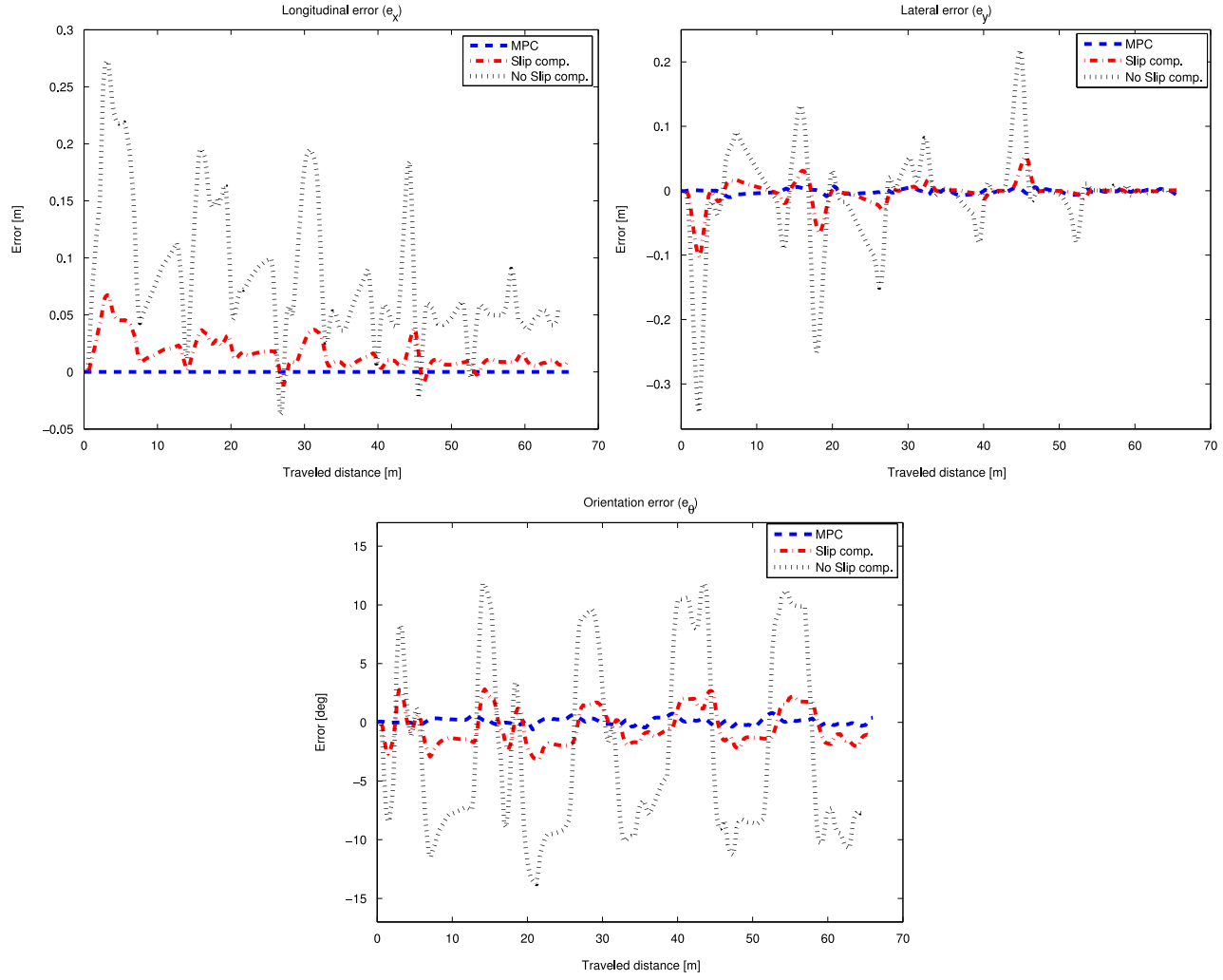

Fig. 4. Longitudinal, lateral, and orientation errors in the simulated experiment.

- For localization purposes, the extended kinematic model (3), which was extended considering slip, was employed. In this case, slip was estimated using a visual-odometry-based approach [33,34]. Visual odometry is defined as the incremental online estimation of robot motion from an image sequence by an on-robot camera [34]. Notice that it means that typical and undesirable effects of wheel-based odometry are minimized, since visual information gives the actual robot

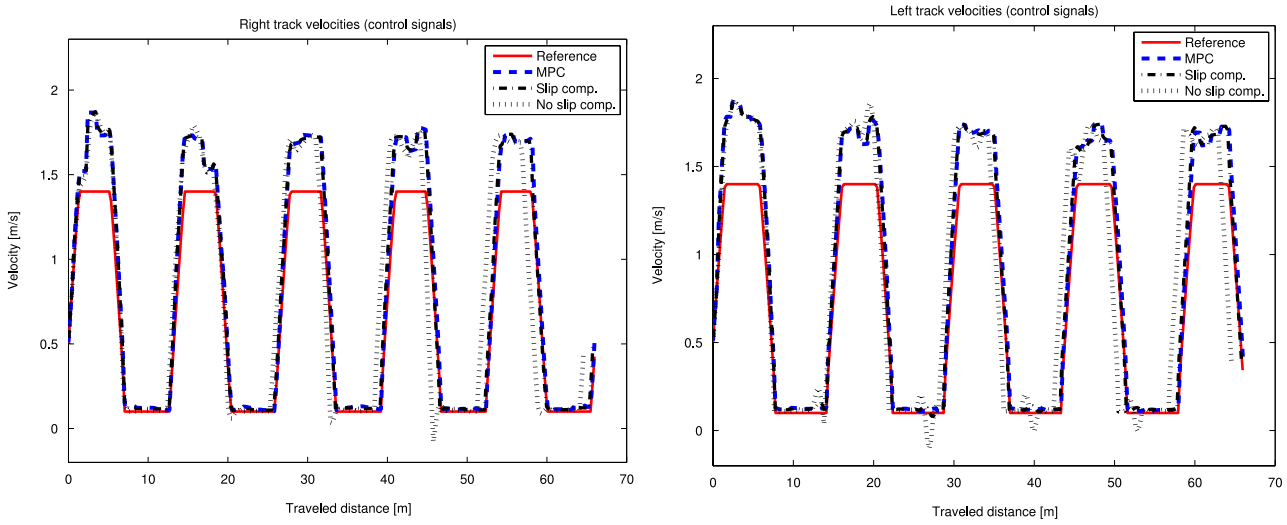

Fig. 5. Control signals (right and left wheel velocities) in the simulated experiment.

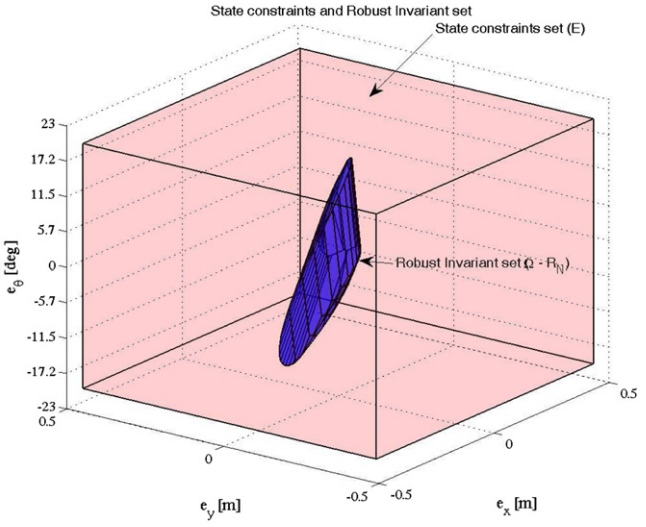

Fig. 6. State constraints and robust invariant set used in the MPC controller for the simulated experiment.

velocity. In particular, a camera pointing at the ground beneath the robot was employed. Visual odometry was implemented using a template matching approach. Furthermore, a threshold filter was employed to attenuate outliers due to mainly false matches [35].

- The tests were carried out on an off-road gravel terrain. Although this is not an ideal site for the experiments, since it is a partially bumpy terrain, the results presented here are illustrative of the performance of the compared controllers. Fig. 8 details the soil of the experiment site. Notice the sinkage effect in both views. This sinkage leads to longitudinal slip.
- The experiments were carried out with sunlit conditions, and thus some shadows that could lead to false matches in the visual odometry algorithm were observed. Nevertheless, these false matches were minimized selecting a proper position for the camera looking at the ground and an appropriate filter.
- In order to validate the followed trajectories and orientations, a DGPS (R100, Hemisphere, Calgary, Canada) and a magnetic compass (C100, KVH, Middletown, USA) have been employed as ground-truth. The DGPS has an accuracy of 0.20 (m) and the magnetic compass of 0.1 (deg). The rest of sensors were: one consumer-grade camera (Quickcam Sphere AF, Logitech, Apples, Switzerland) and two incremental encoders attached to the track drive sprockets (DRS61, Sick AG, Waldkirch, Germany).
- Although many experiments have been carried out, a circular trajectory and an U-shaped trajectory have been selected in this case. In the former, the robot moved at middle/high velocities ($\geq$ 0.5 (m/s)) and in the second one it moved at low velocities

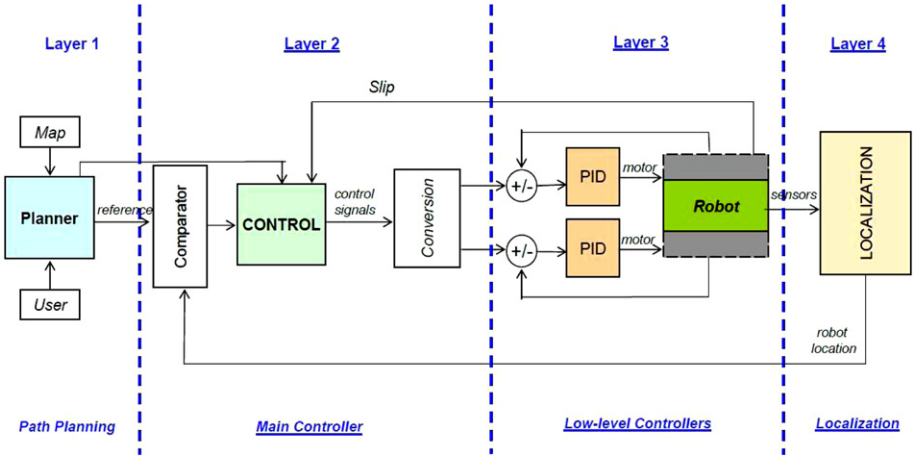

Fig. 7. Control architecture of the testbed.

(a) Robot on gravel terrain. (b) Soil detail.

Fig. 8. Experiment site (gravel soil).

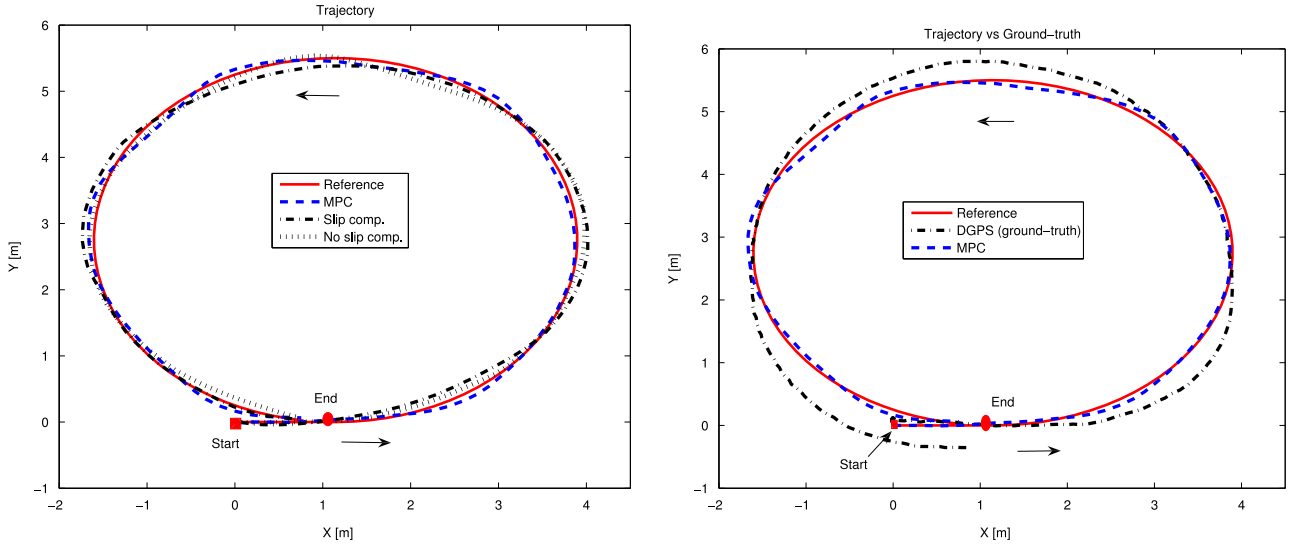

(a) Followed trajectories. (b) MPC-trajectory vs. ground-truth.

Fig. 9. Experiment 1. Followed trajectories during the experiment.

(≤ 0.4 (m/s)). Notice that similar trajectories to these selected here are usually employed in off-road mobile robotics, see for instance [10,36].

The same parameters used for the simulation were employed during the physical experiments.

4.3.1. Experiment 1. Circular trajectory

In this first experiment, a reference circular trajectory was tested. The motivation for selecting this trajectory is because it is a closed trajectory, what helps in a better comparison of the controllers, since the robot has to come back to the starting point. Furthermore, the reference track velocities were 0.6 (m/s) for the right track and 0.5 (m/s) for the left track. For the testbed, these can be considered as middle/high velocities. In this first selected experiment, the total traveled distance was close to 18 (m).

Fig. 9(a) shows the reference trajectory and the followed trajectories using the three control strategies. Fig. 9(b) shows the reference trajectory, the trajectory followed using the MPC controller, and the ground-truth (DGPS). In the former plot, it is possible to observe that the MPC controller achieves the best behavior. From Fig. 9(b), it is possible to notice that there is a small mismatch between the trajectory obtained using the MPC controller and the ground-truth. Nevertheless, the maximum lateral deviation is 0.53 (m), and the mean lateral deviation is 0.18 (m), which means 1 (%) of the total traveled distance. It must bear in mind that since a kinematic model is employed, the error-growth effect of kinematic-model-based solutions is not fully avoided, although it is minimized using the visual odometry approach. This explains why there is a small mismatch between the trajectory followed using the MPC controller and the ground-truth.

Fig. 10(a) displays the orientations of the compared controllers. It can be observed the proper behavior of the MPC controller with few oscillations. Fig. 10(b) plots the reference orientation, the orientation obtained using the MPC controller, and the ground-truth (magnetic compass). As expected from the previous discussion, the orientation obtained using the MPC controllers follows the ground-truth with small deviation. Particularly, the mean deviation is 7.62 (deg).

Fig. 11 shows the slip estimation for each track. Recall that the slip is obtained as the relation between the actual robot velocity (visual odometry) and the theoretical velocities of the tracks (incremental encoders). In this particular experiment, the tracks move at different velocities. For that reason, the obtained slip estimations are different. Notice that this fact can lead to a mistake since the same actual velocity is being supposed for both tracks. In order to minimize this mistake presented in circular trajectories, the mean value of both slip estimations was considered. In further works, two independent cameras will be employed to estimate the actual track velocity. The mean slip is 4.41 (%) (gravel soil).

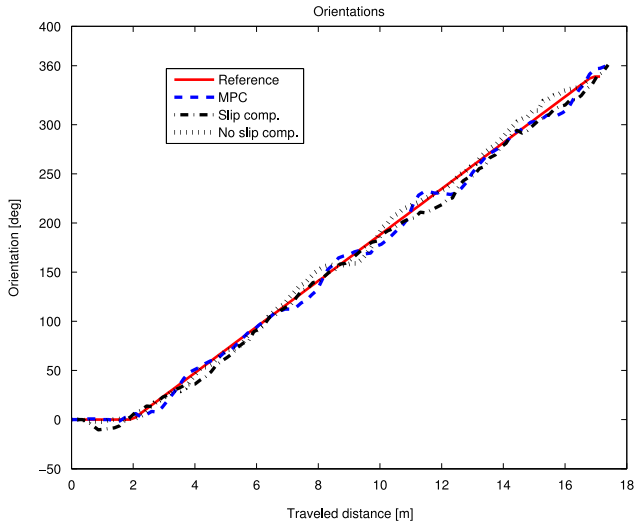

(a) Orientations.

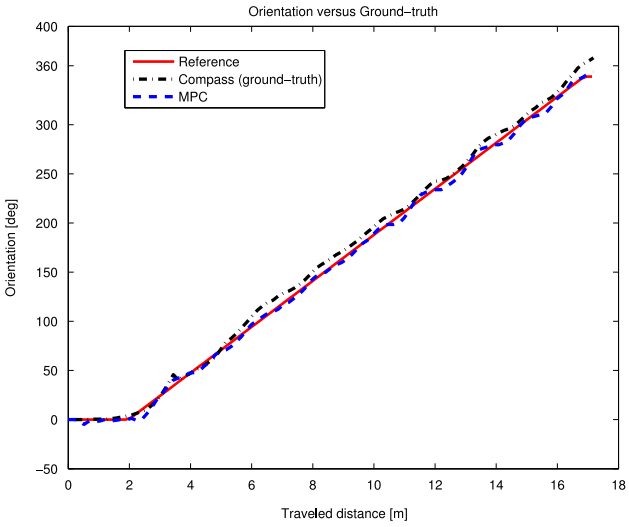

(b) MPC-orientation vs. ground-truth.

Fig. 10. Experiment 1. Orientations.

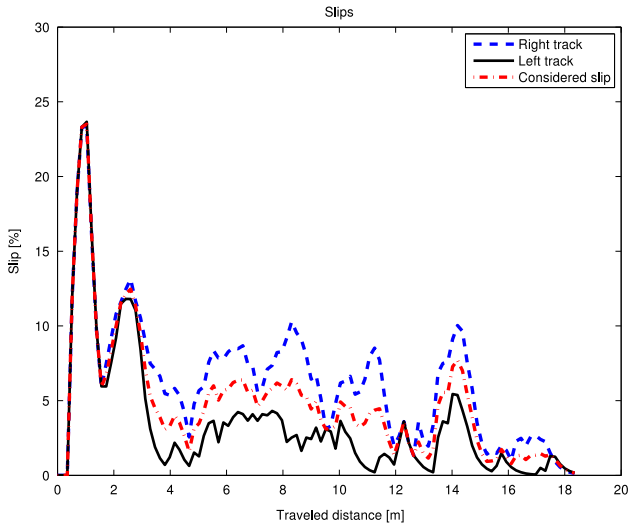

Fig. 11. Experiment 1. Slip estimation for the case of the MPC controller.

The errors between the reference trajectory and those steered by the compared controllers are displayed in Fig. 12. In these plots, the proper behavior of the predictive controller is verified. The slip compensation controller also achieves a satisfactory result in comparison to the no slip compensation controller. As in simulations, a positive longitudinal error is observed. This means that the real robot is pursuing the reference robot. The mean longitudinal errors are: 0.05 (m) with standard deviation 0.05 (m) for the MPC controller, 0.09 (m) with standard deviation 0.10 (m) for the slip compensation controller, and 0.13 (m) with standard deviation 0.10 (m) for the no slip compensation controller. The mean lateral errors are: −0.002 (m) with standard deviation 0.05 (m) for the MPC controller, −0.01 (m) with standard deviation 0.08 (m) for the slip compensation controller, and −0.02 (m) with standard deviation 0.07 (m) for the no slip compensation controller. The mean orientation errors are: 0.50 (deg) with standard deviation 5.80 (deg) for the MPC controller, 1.80 (deg) with standard deviation 4.84 (deg) for the slip compensation controller, and 2.27 (deg) with standard deviation 4.73 (deg) for the no slip compensation controller.

Fig. 13 shows the reference velocities (denoted as v_r^{rf} and v_l^{rf}), the control inputs (referred to as v_r and v_l), and the real track velocities (labeled as "Right Enc." and "Left Enc.") for the case of the MPC controller. As in simulation, the motion controller increases the control inputs to compensate the negative slip effect. It is interesting to point out the proper behavior of the low-level PI controllers, which are responsible to achieve the set-points given by the motion controllers.

Finally, Fig. 14(a) displays the pixel displacement values between consecutive images for the case of the MPC controller (visual odometry), and the computation time employed (CPU time employed at each sampling instant) by the MPC controller and the slip compensation controller. It is important to remark that since the robot is moving on a circular trajectory, different lighting conditions occurred during the motion. This situation leads to shadows in the images employed by the visual odometry approach, which are used to estimate the actual robot velocity. However, as shown in Fig. 14(a), an admissible number of outliers takes place, due to the proper downward camera position and the threshold filter. Fig. 14(b) shows the low computation time employed by the slip compensation controllers. Furthermore, it is checked that sampling period is always ensured. In this case, the mean computation time for the MPC controller is 0.25 (s) and for the slip compensation controller is 0.20 (s) (the no slip compensation controller achieves a similar value). Notice that motion controllers run on the computer on-board the mobile robot (Intel Pentium III 1 GHz, 512 MB RAM).

4.3.2. Experiment 2. U-shaped trajectory

In this second experiment, an U-shaped trajectory has been selected. It constitutes an interesting trajectory which combines straight-line motions and two 90° turns. The total traveled distance was close to 30 (m). In order to check the navigation architecture at low velocities, a maximum reference velocity of 0.3 (m/s) was selected.

Fig. 15(a) shows the reference trajectory and the followed trajectories using the three control strategies. Fig. 15(b) displays the reference trajectory, the trajectory followed using the predictive controller and the ground-truth (DGPS). In the former plot, it is possible to observe that the trajectory obtained using the predictive controller follows satisfactorily the reference. The trajectories obtained using the linear feedback controllers have an smooth oscillatory behavior, especially after the 90° turns. As in the previous experiment, the trajectory followed using the predictive controller slightly diverges from ground-truth. Particularly, the

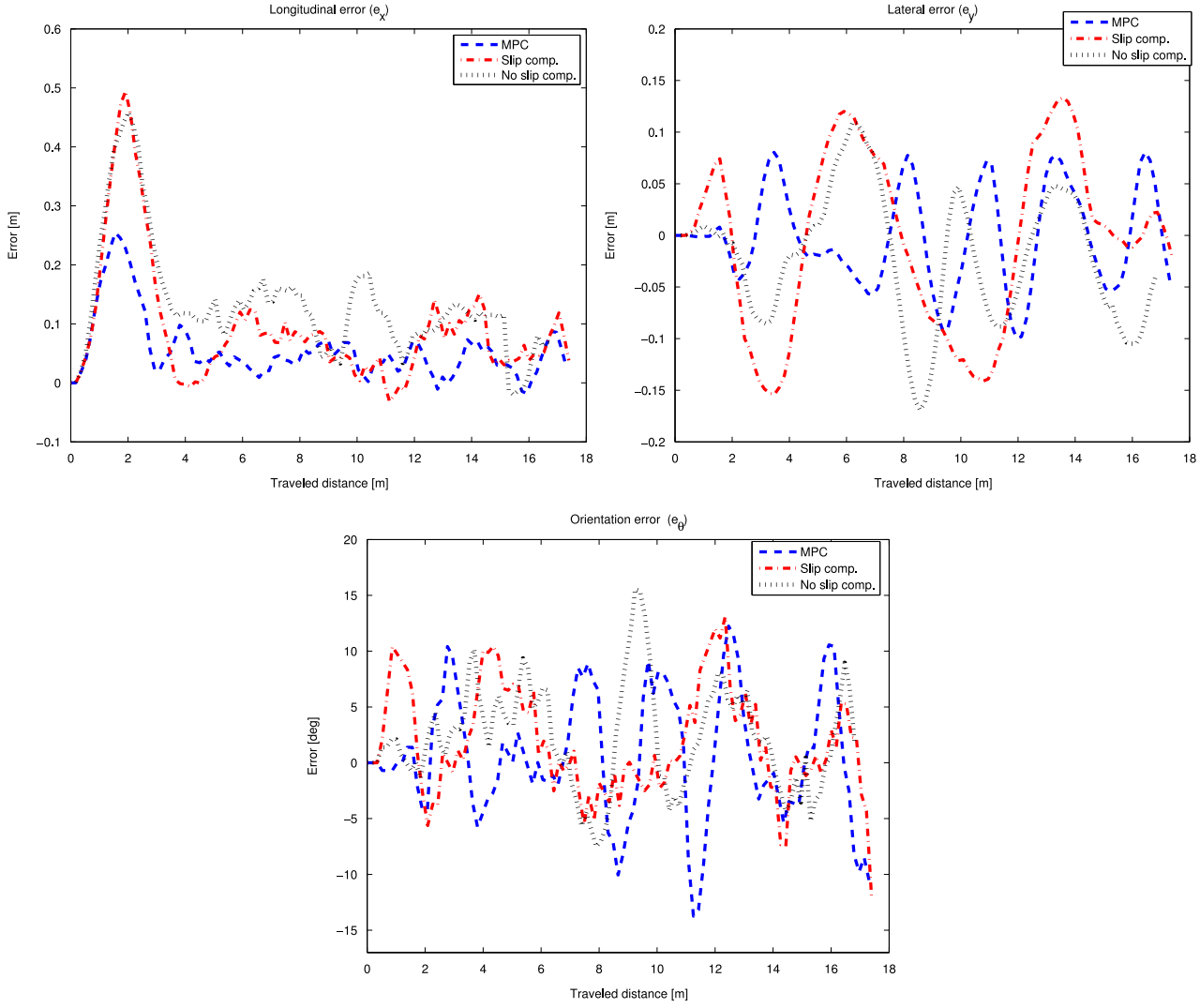

Fig. 12. Experiment 1. Longitudinal, lateral, and orientation errors in the physical experiment.

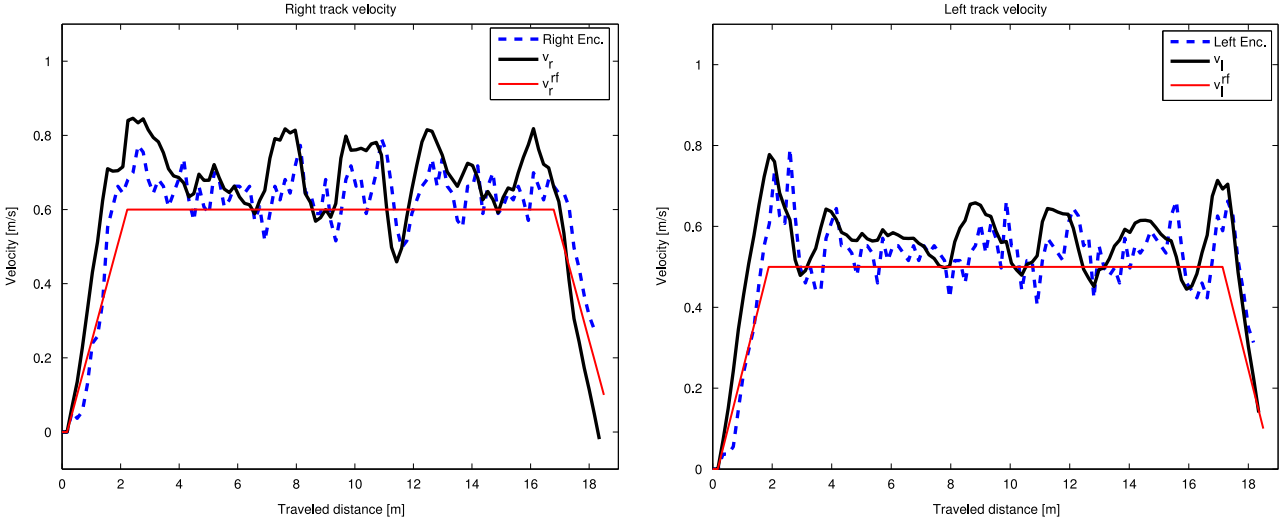

(a) Right track. (b) Left track.

Fig. 13. Experiment 1. Control signals (track velocities) in the physical experiment.

maximum lateral deviation is 0.72 (m), and the mean lateral deviation is −0.11 (m), what means 0.40 (%) of the total traveled distance.

Fig. 16(a) shows the orientations. From this figure, it is clearly observed the smooth oscillatory behavior of the linear feedback controllers, especially at the end of the experiment. The orientation

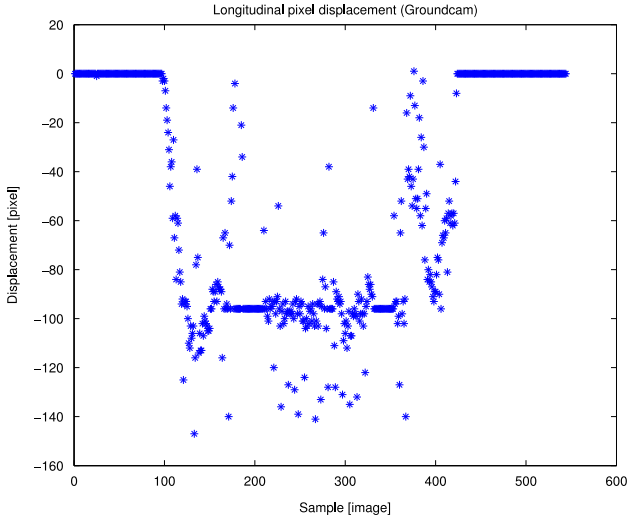

(a) Visual odometry data.

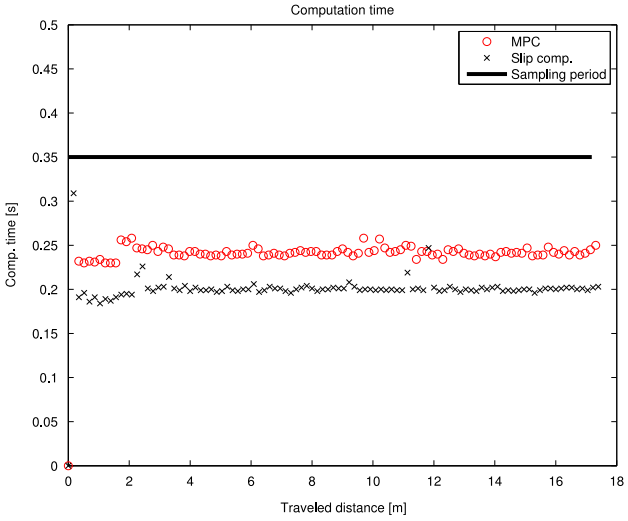

(b) Computation time.

Fig. 14. Experiment 1. Pixel displacements (MPC controller) and computation time (MPC vs. Slip comp. controllers).

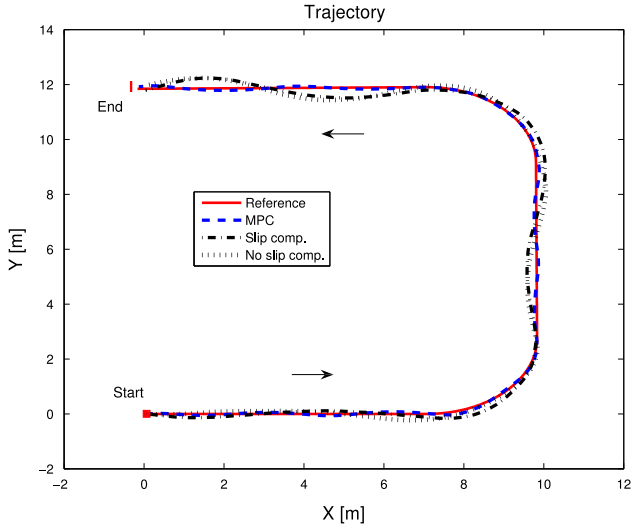

(a) Followed trajectories.

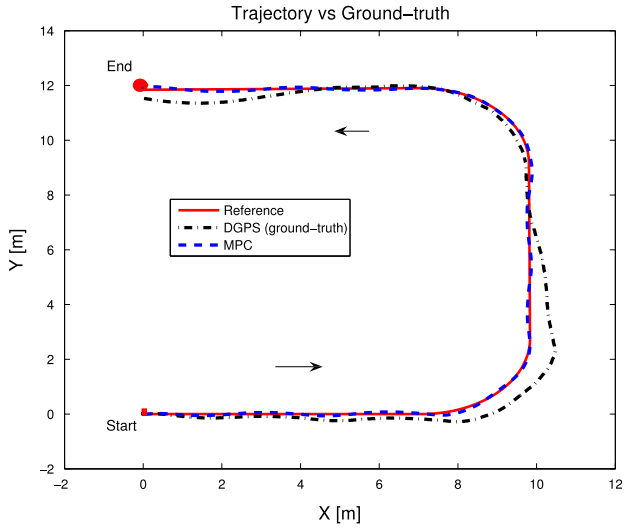

(b) MPC-trajectory vs. ground-truth.

Fig. 15. Experiment 2. Followed trajectories during the experiment.

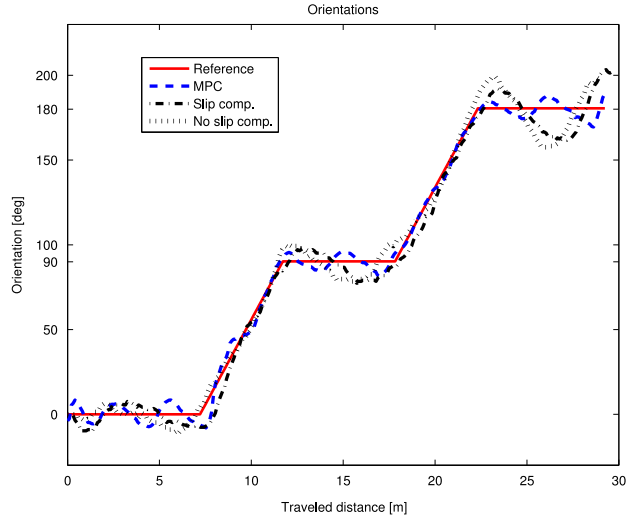

(a) Orientations.

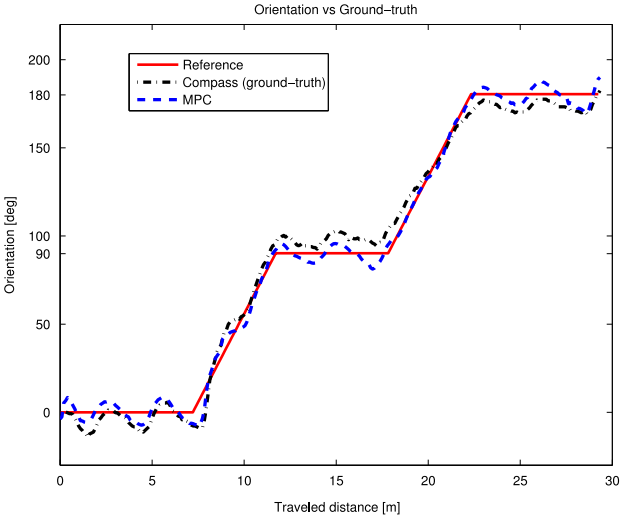

(b) MPC-orientation vs. ground-truth.

Fig. 16. Experiment 2. Orientations.

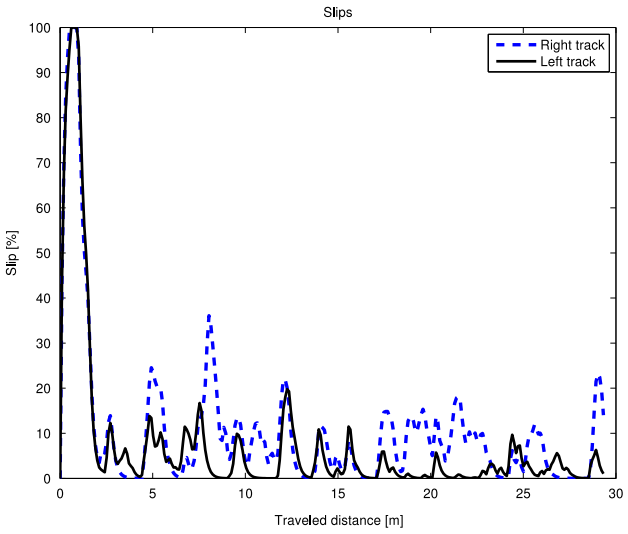

Fig. 17. Experiment 2. Slip estimation for the case of the MPC controller.

obtained using the predictive controller follows the reference with very small oscillations. Fig. 16(b) plots the reference orientation, the orientation obtained using the predictive controller, and the ground-truth (magnetic compass). As expected, the orientation obtained using the predictive controller does not fix the ground-truth. In this case, the mean deviation is −0.11 (deg) with standard deviation 6.47 (deg).

Fig. 17 displays the slip estimations. In this case, the median slip value for the right track was 6.32 (%), and for the left track was 2.17 (%). As in previous experiment, both slip values are different and the reason is that the same actual velocity has been used for both tracks.

The errors between the reference trajectory and those steered by the compared controllers are plotted in Fig. 18. Especially remarkable is the almost zero lateral error achieved by the MPC controller. The mean longitudinal errors are: 0.02 (m) with standard deviation 0.03 (m) for the MPC controller, 0.09 (m) with standard deviation 0.05 (m) for the slip compensation controller, and 0.13 (m) with standard deviation 0.06 (m) for the no slip compensation controller. The mean lateral errors are: 0 (m) with standard deviation 0.04 (m) for the predictive controller, 0.02 (m) with standard deviation 0.17 (m) for the slip compensation controller, and 0.01 (m) with standard deviation 0.18 (m) for the no slip compensation controller. The mean orientation errors are: 0.43 (deg) with standard deviation 4.74 (deg) for the MPC controller, 0.66 (deg) with standard deviation 8.16 (deg) for

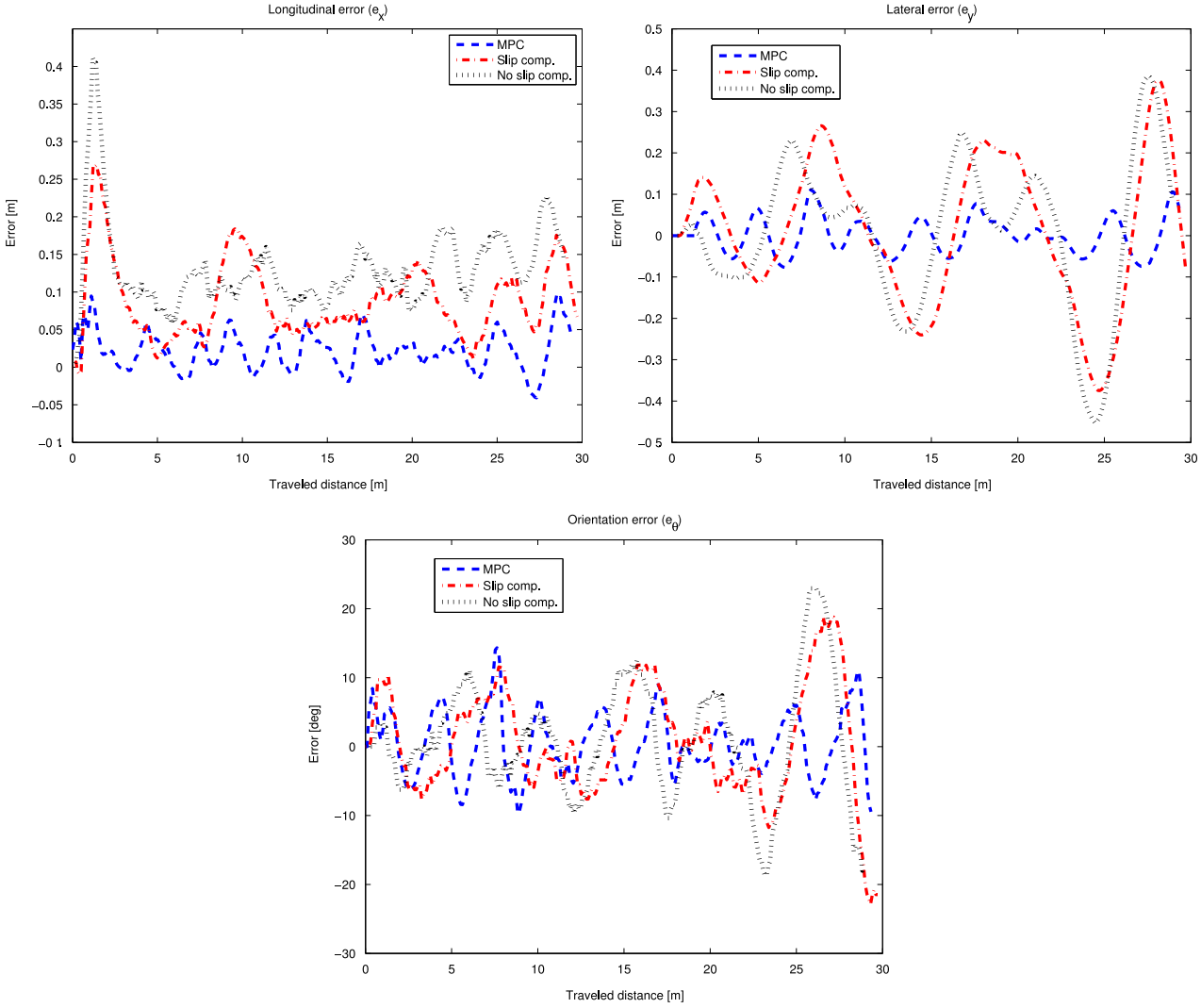

Fig. 18. Experiment 2. Longitudinal, lateral, and orientation errors in the physical experiment.

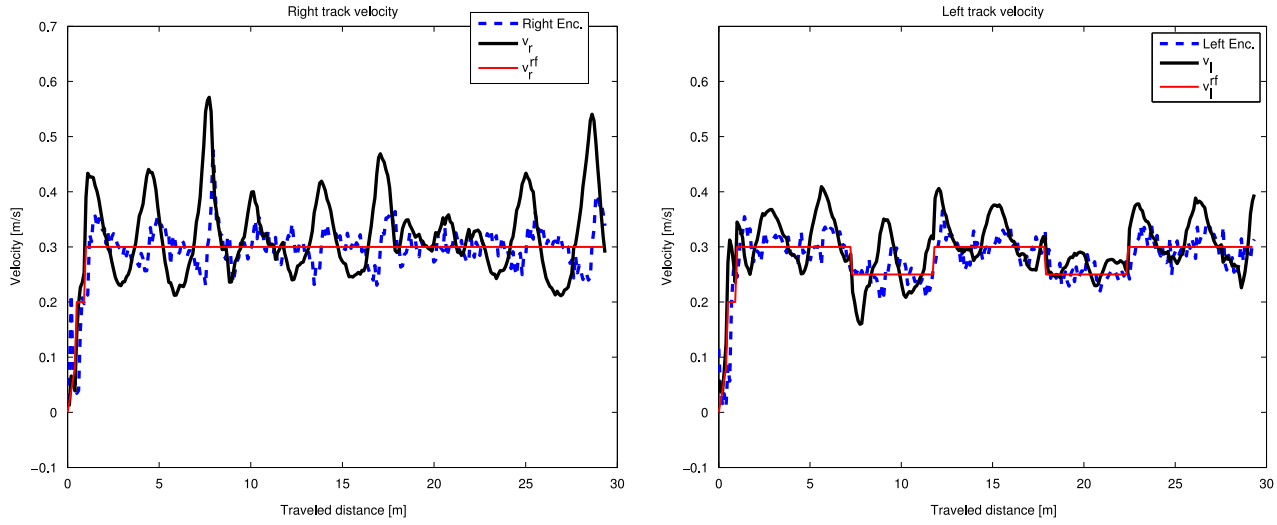

(a) Right track. (b) Left track.

Fig. 19. Experiment 2. Control signals (track velocities) in the physical experiment.

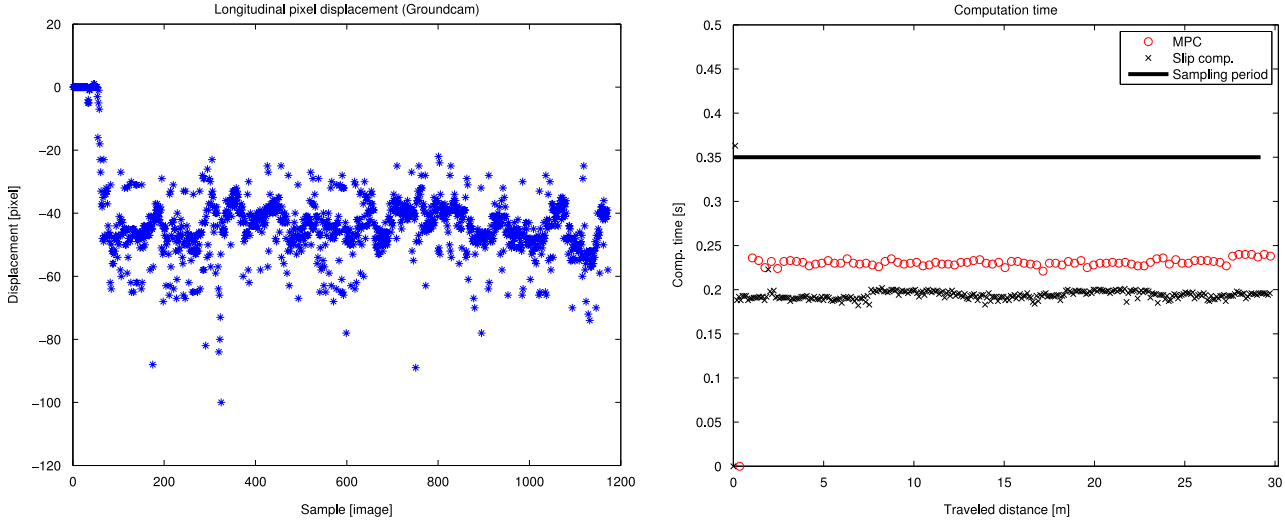

(a) Visual odometry data. (b) Computation time.

Fig. 20. Experiment 2. Pixel displacements (MPC controller) and computation time (MPC vs. Slip comp. controllers).

the slip compensation controller, and 1.09 (deg) with standard deviation 8.51 (deg) for the no slip compensation controller. As in the previous experiment, the predictive control strategy obtains the best results. Furthermore, note that the rest of compared controllers oscillate between maximum values closer or greater to 0.3 (m), which could be unacceptable for some kind of applications.

Fig. 19 displays the reference velocities, the control inputs and the real track velocities for the case of the predictive controller. These plots notice the proper tuning of the PI controllers, since the real velocities of the tracks follow satisfactorily the set-points. It is important to clarify that the smooth oscillatory behavior of the right track is stressed by that fact that the mobile robot was moving on a partially bumpy gravel soil. In this scenario, little stones produce vibrations to the vehicle, and hence to the tracks. Notice that in the previous experiment, a similar behavior was observed.

Finally, Fig. 20(a) displays the pixel displacement between consecutive images for the MPC controller (visual odometry). As in previous experiment, few outliers appear due to the proper downward camera position and the threshold filter. Notice that in this experiment the mean value of the pixel displacement is around −50 (pixel). This confirms that the mobile robot was moving at a slower velocity than in previous experiment. Fig. 20(b) shows the computation time employed by the predictive controller and the slip compensation controller. The average computation time for the predictive controller is 0.24 (s) and for the slip compensation controller is 0.19 (s) (the no slip compensation controller achieves a similar value).

5. Conclusions

This paper proposes a robust tube-based predictive control law for constrained mobile robots in off-road conditions.

From the theoretical point of view, an extension of tube-based predictive control to time-varying systems is provided (via reachable sets). From a practical point of view, the designed control strategy compensates slip and guarantee that state and input constraints are fulfilled, since these constraints are taken into account in the solution of the optimization problem. The time-varying trajectory tracking error model with additive uncertainties has been addressed. Real-time execution has been ensured using tube-based MPC formulation and it has been tested through simulations and physical experiments. The comparative study (simulations and physical experiments) with other control laws illustrates the proper behavior of the robust tube-based MPC strategy.

Summing up, the main advantages of the proposed control scheme are: robustness, efficient online computation, state and input constraints fulfillment and compensation of longitudinal slip. It is interesting to point out that the proposed approach can be easily applied to other robot configurations. The main limitation of the current strategy is a certain degree of conservativeness, mainly related to calculation of reachable sets. Then, future efforts will be devoted to reduce such degree of conservatism. Furthermore, a more precise estimation of the uncertainty set W and new physical experiments will be tested.

Acknowledgments

This work has been supported in part by the Spanish CICYT under grants DPI 2007-66718-C04-01, DPI 2007-66718-C04-04, and DPI2010-21589-C05-04. The authors would like to thank professors R. Siegwart and C. Pradalier from the Autonomous System Lab, ETH Zürich (Switzerland) for introducing us the visual odometry localization technique.

Appendix. Robust positively terminal invariant set

In what follows, once a stabilizing control law is given, we provide a procedure to obtain the maximal robust invariant set for the uncertain system (trajectory tracking error model with slip) contained in the state constraint set. In addition, constraints on the input are considered.

Let $A_\gamma \in \mathscr{A}$, with $\mathscr{A}$ a polytope in $\mathbb{R}^{3\times 3}$ holds for the system (7), and the input to be constrained, $u(k) \in U$. Given a control feedback gain $\kappa(A_\gamma) = \lambda_1\kappa^1(A_\gamma^1)+\cdots+\lambda_4\kappa^4(A_\gamma^4)$ (each gain is calculated in (42)), and a convex set $\Omega \subseteq \mathbb{R}^3$, the concept of one-step operator is employed as

$$Q_{\mathscr{A}}(\Omega) = \{e \in E : \kappa(A_\gamma)e \in U, (A_\gamma + B_d\kappa(A_\gamma))e + w \in \Omega,\ \forall w \in W,\ \forall A_\gamma \in \mathscr{A}\}.$$

Notice that the one-step operator is a standard tool for the invariant sets calculation through iterative procedures [18]. Parameters λ_j with $j = 1, \ldots, 4$, can be obtained by solving a linear programming problem (LP).

Finally, taking into account the one-step operator previously defined, the maximal robust invariant set for the uncertain system (7) is obtained by means of the following iterative procedure:

1. Initialization: $\Omega_0 = E \cap \{\omega \in \mathbb{R}^3 : \kappa(A_\gamma)\omega \in U,\ \forall A_\gamma \in \mathscr{A}\}$.
2. Iteration: $\Omega_{k+1} = \Omega_k \cap Q_{\mathscr{A}}(\Omega_k)$.
3. Termination condition: stop when $\Omega_{k+1} = \Omega_k$ or $\Omega_{k+1} = \emptyset$. Set $\Omega = \Omega_\infty = \Omega_{k+1}$.

An important issue when dealing with algorithmic procedure for computing the robust invariant sets is its finite determinedness, that is, the conditions under which the algorithm provides a solution after a finite number of iterations. Results regarding the problem of finite determination can be found in [18,17]. Finite determinedness has not been proved for this work, since it goes beyond the aim of the paper. Nevertheless, the application of the algorithm to the case under analysis provides a result after a finite number of iterations.

References

[1] D. Mayne, J. Rawlings, C. Rao, P. Scokaert, Constrained model predictive control: stability and optimality, Automatica 36 (6) (2000) 789–814.
[2] E. Camacho, C. Bordons, Model Predictive Control, second ed., in: Advanced Textbooks in Control and Signal Processing, Springer, Germany, 2007.
[3] A. Bemporad, F. Borrelli, M. Morari, Model predictive control based on linear programming—the explicit solution, IEEE Transactions on Automatic Control 47 (12) (2002) 1974–1985.
[4] A. Bemporad, M. Morari, Robust model predictive control: a survey, in: A. Garulli, A. Tesi, A. Vicino (Eds.), Robustness in Identification and Control, Springer, Germany, 1999, pp. 207–226.
[5] P. Scokaert, D. Mayne, Min–max feedback model predictive control for constrained linear systems, IEEE Transactions on Automatic Control 43 (8) (1998) 1136–1142.
[6] J. Wong, Theory of Ground Vehicles, third ed., John Wiley & Sons, Inc., USA, 2001.
[7] R. González, M. Fiacchini, T. Álamo, J. Guzmán, F. Rodríguez, Adaptive control for a mobile robot under slip conditions using an LMI–based approach, European Journal of Control 16 (2) (2010) 144–155.
[8] D. Wang, C. Low, Modeling and analysis of skidding and slipping in wheeled mobile robots: control design perspective, IEEE Transactions on Robotics 24 (3) (2008) 676–687.
[9] C. Cariou, R. Lenain, B. Thuilot, M. Berducat, Automatic guidance of a four-wheel-steering mobile robot for accurate field operations, Journal of Field Robotics 26 (6–7) (2009) 504–518.
[10] A. Le, Modelling and control of tracked vehicles, Ph.D. Thesis, University of Sydney, Sydney, Australia, 1999.
[11] G. Klancar, I. Skrjanc, Tracking-error model-based predictive control for mobile robots in real time, Robotics and Autonomous Systems 55 (1) (2007) 460–469.
[12] J. Gómez, E. Camacho, Mobile robot navigation in a partially structured static environment, using neural predictive control, Control Engineering Practice 4 (12) (1996) 1669–1679.
[13] J. Normey-Rico, J. Gómez-Ortega, E. Camacho, A smith-predictor-based generalised predictive controller for mobile robot path-tracking, Control Engineering Practice 7 (6) (1999) 729–740.
[14] D. Ramírez, T. Álamo, E. Camacho, D.M. de la Peña, Min–max MPC based on a computationally efficient upper bound of the worst case cost, Journal of Process Control 16 (5) (2006) 511–519.
[15] L. Chisci, J. Rossiter, G. Zappa, Systems with persistent disturbances: predictive control with restricted constraints, Automatica 37 (7) (2001) 1019–1028.
[16] W. Langson, I. Chryssochoos, S. Rakovic, D. Mayne, Robust model predictive control using tubes, Automatica 40 (1) (2004) 125–133.
[17] F. Blanchini, Set invariance in control, Automatica 35 (11) (1999) 1747–1767.
[18] I. Kolmanovsky, E. Gilbert, Theory and computation of disturbance invariant sets for discrete-time linear systems, Mathematical Problems in Engineering 4 (4) (1998) 317–367.
[19] C. Canudas, B. Siciliano, G. Bastin, Theory of Robot Control, second ed., in: Communications and Control Engineering, Springer, Germany, 1997.
[20] G. Campion, G. Bastin, B.D. Andréa-Novel, Structural properties and classification of kinematic and dynamic models of wheeled mobile robots, IEEE Transactions on Robotics and Automation 12 (1) (1996) 47–62.
[21] R. González, F. Rodríguez, J. Guzmán, M. Berenguel, Localization and Control of Tracked Mobile Robots Under Slip Conditions, in: IEEE International Conference on Mechatronics, IEEE, Málaga, Spain, 2009.
[22] R. Lenain, B. Thuilot, C. Cariou, P. Martinet, Adaptive and predictive path tracking control for off-road mobile robots, European Journal of Control 13 (4) (2007) 419–439.
[23] K. Aström, R. Murray, Feedback Systems: An Introduction for Scientists and Engineers, Princeton University Press, USA, 2008.
[24] D. Limón, T. Álamo, E. Camacho, Input-to-state Stable MPC for Constrained Discrete–time Nonlinear Systems with Bounded Additive Uncertainties, in: IEEE Conference on Decision and Control, IEEE, Las Vegas, USA, 2002, pp. 4619–4624.
[25] A. Bemporad, M. Morari, V. Dua, E. Pistikopoulos, The explicit linear quadratic regulator for constrained systems, Automatica 38 (1) (2002) 3–20.
[26] D. Limón, J. Bravo, T. Álamo, E. Camacho, Robust MPC of constrained nonlinear systems based on interval arithmetic, IET Control Theory & Applications 152 (3) (2005) 325–332.
[27] S. Boyd, L.E. Ghaoui, E. Feron, V. Balakrishnan, Linear Matrix Inequalities in System and Control Theory, Society for Industrial and Applied Mathematics, USA, 1994.
[28] M. Kothare, V. Balakrishnan, M. Morari, Robust constrained model predictive control using linear matrix inequalities, Automatica 32 (10) (1996) 1361–1379.
[29] P. Gahinet, A. Nemirovski, A. Laub, M. Chilali, LMI Control Toolbox User's Guide, first ed., The MathWorks, Inc., USA, 1995.
[30] M. Kvasnica, P. Grieder, M. Baotić, Multi-parametric toolbox, MPT, 2004. http://control.ee.ethz.ch/mpt/.

[31] R. González, F. Rodríguez, J. Sánchez-Hermosilla, J. Donaire, Navigation techniques for mobile robots in greenhouses, Applied Engineering in Agriculture 25 (2) (2009) 153–165.
[32] G. Dudek, M. Jenkin, Computational Principles of Mobile Robotics, 1st ed., Cambridge University Press, United Kingdom, 2000.
[33] A. Angelova, L. Matthies, D. Helmick, P. Perona, Learning and prediction of slip from visual information, Journal of Field Robotics 24 (3) (2007) 205–231.
[34] L. Matthies, Dynamic stereo vision, Ph.D. Thesis, Carnegie Mellon University, Pittsburgh, USA, 1989.
[35] R. González, Localization of the CRAB rover using visual odometry, Tech. Rep., Autonomous Systems Lab, ETH Zürich, Switzerland, December 2009. http://www.ual.es/personal/rgonzalez/english/publications.htm.
[36] R. Lenain, B. Thuilot, C. Cariou, P. Martinet, Mixed kinematic and dynamic sideslip angle observer for accurate control of fast off-road mobile robots, Journal of Field Robotics 27 (2) (2010) 181–196.

Ramón González obtained a Computer Science Engineering degree in 2006 and an European Ph.D. in 2011, both from the University of Almería, Spain. Currently, he holds a research fellowship from the Spanish Ministry of Education. He has participated in several Spanish and European projects. His research interests are in motion control of mobile robots in off-road conditions; adaptive, predictive and robust control applied to mobile robotics; localization techniques for off-road mobile robots; and space and agriculture robots.

Mirko Fiacchini was born in Italy in 1977. He received the Laurea degree in Computer Science Engineering in 2004 from the University of Florence and the Ph.D. in Control Engineering from University of Seville in 2010. He was working as visiting Ph.D. student at ETH of Zurich (Switzerland). He is currently postdoctoral researcher at LAAS-CNRS, Toulouse, France. He has participated in several Spanish and European Projects, and his current research interests are in Model Predictive Control, robust control, set-theory in control and invariant sets.

José Luis Guzmán is Associate Professor of Automatic Control and System Engineering at the University of Almería (Spain), where he earned a computer science engineering degree in 2002 and an European Ph.D. in 2006 (extraordinary doctorate award). He is also researcher of the Automatic control, Electronics, and Robotics group at University of Almería. His research interests are focused on the field of control education, model predictive control techniques, robust control, and PID control, with applications to agricultural processes, solar plants, and biotechnology. He has authored and coauthored more than 80 technical papers in international journals and conferences. He is member of IEEE Control System Society from 2006, of the IFAC Technical Committee on Control Education from 2008, and of the IEEE Technical Committee on System Identification and Adaptive Control from 2008.

Teodoro Álamo was born in Spain in 1968. He received his M.Eng. degree in Telecommunications Engineering from the Polytechnic University of Madrid (Spain) in 1993 and his Ph.D. in Telecommunications Engineering from the University of Seville in 1998. From 1993 to 2000 he was assistant professor of the Department of System Engineering and Automatic Control of the University of Seville. Since 2001, he has been associate professor and since 2010 he is full professor in the same department. He was a Researcher in the Ecole Nationale Supérieure des Télécommunications (Telecom Paris) from 1991 to 1993 and he has participated in several European Projects. He is the author or coauthor of more than 120 publications including book chapters, journal papers, conference proceedings and educational books. He has carried out reviews for various conferences and technical journals. His current research interests are in model predictive control, randomized algorithms, robust control, identification, control of constrained systems, invariant sets and convex optimization.

Francisco Rodríguez is Associate Professor of Systems Engineering and Automatic Control at the University of Almería (Spain). He obtained his Telecommunication Engineering degree from Madrid Polytechnics University (Spain) and his Ph.D. degree from the University of Almería in 2002. Now he is a researcher and member of the Automatic Control, Electronics, and Robotics group of the University of Almería. He has participated in several Spanish and European Projects, and his current research interests are focused to the application of modelling, automatic control, and robotics techniques to agricultural systems and education.